Acta Chemica Scandinavica, 1997: 51: 910–917
Printed in UK – all rights reserved

ACTA
CHEMICA SCANDINAVICA
ISSN 0904-213X

Structural and Magnetic Properties of the Chemical Pressure System $Mn_{0.64}Cr_{0.36}As_{1-x}Sb_x$

Helmer Fjellvåg* and Arne Kjekshus

Department of Chemistry, University of Oslo, N-0315 Oslo, Norway

Fjellvåg, H. and Kjekshus, A., 1997. Structural and Magnetic Properties of the Chemical Pressure System $Mn_{0.64}Cr_{0.36}As_{1-x}Sb_x$. – Acta Chem. Scand. 51: 910–917. © Acta Chemica Scandinavica 1997.

The pseudobinary $Mn_{0.64}Cr_{0.36}As$ phase forms a complete solid solution when As is substituted by Sb; $Mn_{0.64}Cr_{0.36}As_{1-x}Sb_x$ with $0.00 \leqslant x \leqslant 1.00$. The introduction of Sb on As sites causes volume expansion. The orthorhombic MnP-type deformation is thereby decreased towards zero, and the crossover from MnP- to hexagonal NiAs-type structure occurs at $x_D = 0.135 \pm 0.005$ for $T = 298$ K. A combined structural and magnetic phase diagram is given. Comparison is made with $Mn_{0.64}Cr_{0.36}As_{1-x}P_x$ where the distorted MnP-type phase becomes stabilized by introduction of phosphorus. The substitution of P or Sb for As causes structural changes which parallel $Mn_{0.64}Cr_{0.36}As$ subjected to positive or negative external pressures, respectively. The effects of chemical pressure are further manifested in the magnetic properties. The structural and magnetic properties have been studied by powder X-ray and neutron diffraction and by magnetization studies. The double, incommensurate, H_a-type helix mode found in $Mn_{0.64}Cr_{0.36}As$ at low temperatures is destabilized on Sb-substitution. Instead the H_c-type helix is favoured, which is a reflection of the volume requirements of the different magnetic modes. In the composition range of the NiAs-type phase, a ferromagnetic structure occurs at low temperatures, which at still higher Sb contents is converted into a ferrimagnetic state with an appreciable antiferromagnetic component. The variations in structural and magnetic properties are discussed on the basis of the concept of chemical pressure introduced on homovalent non-metal substitution.

The $Mn_{1-t}Cr_tAs$ pseudobinary solid-solution phase has been extensively studied owing to its richness of interesting structural and magnetic properties.[1–15] The most intriguing features are found in the composition interval $\sim 0.30 < t < \sim 0.50$, where para- (P; either NiAs- or MnP-type crystal structure; the spin state for the latter varying between 'low' and 'high' spin), antiferro- (H_a or H_c double-spiral structure with propagation direction along a_{MnP} or c_{MnP}, respectively) and ferromagnetic (F) phases appear depending on composition (t), temperature (T), applied pressure (P) and magnetic field (H). A number of phase transitions are induced by rather modest perturbations and detailed phase diagrams have been traced out.[2,5–8,14,15] Special interest has been devoted to multicritical points where the paramagnetic phase adjoins to two magnetically ordered phases (F, H_a or H_c).[15]

The relative stabilities of the structural and magnetic phases appear to be very sensitive to the unit-cell volume. Interesting transformation schemes are revealed as a function of either externally applied or internally produced chemical pressure.[4,5,14,15] In many respects the two sources of pressure have almost identical impact on the physical properties.

With respect to structural properties, the orthorhombically deformed MnP-type variant of the hexagonal NiAs-type structure is favoured by pressure (or reduced unit-cell volume). For $Mn_{1-t}Cr_tAs$ this implies that the transition temperature T_D for the second-order MnP $\rightleftharpoons$ NiAs-type phase transition increases almost linearly with t from 390 K for MnAs to 1170 K for CrAs.[2] At temperatures below T_D the distortion increases progressively, with respect to both the $(c/b)_{MnP}$ axial ratio and to atomic displacements within the unit cell.

The ordered magnetic phases are characterized by slightly different crystallographic unit-cell volumes (for the same chemical composition). The F- and H_a-type states have a lower volume than the P-state, whereas the H_c-type has a higher unit-cell volume, see Refs. 1–15. This implies that the F- and H_a-types are favoured by pressure. The behaviour of each of the two helimagnetic phases differs strongly when subjected to a magnetic field. The H_c-type is profoundly antiferromagnetic, whereas the H_a-type is nearly ferromagnetic, which in turn can be rationalized when considering spiral periodicities and phase differences between independent

* To whom correspondence should be addressed.

spirals.[1,7] The distinction is further substantiated by the very low magnetic fields which are required for triggering the H_a- to F-type transition.[15]

The strong coupling between crystal structure and magnetic properties implies that MnAs is a good model substance for testing the degree of equivalence between external and internal pressure.[5] It is likely that a related model behaviour will be found in the entire manganese-rich part of the $Mn_{1-t}Cr_tAs$ solid-solution phase. Increasing phosphorus substitution in $Mn_{0.64}Cr_{0.36}As_{1-x}P_x$ causes reduction in the unit-cell volume (V)[14] and crossover from antiferromagnetic (H_c- via H_a-type) to ferromagnetic properties.[14,15] On the other hand, Sb substitution for As will imply a volume increase, which naturally has no counterpart in applied external pressure. The (formal) number of valence electrons is not affected by the substitution since P, As and Sb all belong to main group V. Hence, for the $Mn_{1-t}Cr_tAs_{1-x}X_x$, X = P and Sb, solid-solution system, the chemical pressure produced by the substituents is believed to be the major factor ruling the structural and magnetic properties. This paper presents new results for $Mn_{0.64}Cr_{0.36}As_{1-x}Sb_x$ which are discussed in relation to published data for $Mn_{1-t}Cr_tAs$ and $Mn_{0.64}Cr_{0.36}As_{1-x}P_x$.

Experimental

Small- (0.5–1.0 g) and large-scale (20 g) samples of the solid-solution phase $Mn_{0.64}Cr_{0.36}As_{1-x}Sb_x$, $0.00 \leqslant x \leqslant 1.00$, were prepared by reacting the elements (Mn, 99.99%, crushed flakes, Johnson Matthey; Cr, 99.999%, crushed flakes; As, 99.99%, lumps; Sb, 99.999%, lumps, all Koch Light) in evacuated, sealed silica-glass ampoules. The temperature was slowly increased to 950 °C over 5 days, and kept at this temperature for another 5 days before cooling to room temperature. After careful intermediate grindings, the samples were reannealed twice at 950 °C for 1 week. The samples were finally annealed at 700 °C for 2 weeks and cooled to room temperature over 1 day.

All samples were characterized by powder X-ray diffraction (PXD; Guinier–Hägg cameras, Cu $K\alpha_1$ or Cr $K\alpha_1$ radiation, Si as internal standard). Low- and high-temperature PXD experiments were carried out between 110 and 1200 K with a Guinier–Simon (Enraf–Nonius) camera. The samples were kept inside rotating, sealed and evacuated silica-glass capillaries. The temperature change was synchronized with the movement of the film cassette. Unit-cell dimensions were obtained by least-squares refinements using the CELLKANT program.[16]

Powder neutron diffraction (PND) data were collected with the OPUS III two-axis diffractometer at the JEEP II reactor, Kjeller. Monochromatized neutrons of wavelength 187.7 pm were obtained by reflection from Ge(111). Diffraction data were collected between 2Θ = 5 and 100° in steps of 0.05°. The temperature was varied between 10 and 300 K using a Displex cooling device, and the temperature was controlled and regulated within ±0.5 K with a Thor 3010 controller. The Hewat version[17] of the Rietveld program[18] was used in fitting instrumental and structural parameters. The scattering amplitudes $b_{Mn} = -3.73$, $b_{Cr} = 3.635$, $b_{Sb} = 5.641$ and $b_{As} = 6.58$ fm were used.[19] The metal and non-metal atoms were assumed to be randomly distributed over the respective sublattices. Magnetic formfactors for Mn^{3+} and Cr^{3+} were taken from Ref. 20.

Differential scanning calorimetry (DSC) measurements were performed between 110 and 870 K using a Mettler TA 3000 system at a heating rate of 10 K min^{-1}. Data reduction was performed with standard programs for the system.

Magnetic susceptibility measurements were carried out between 77 and 950 K according to the Faraday method (maximum field 8 kOe, 5–20 mg samples), and between 4 and 300 K using a SQUID magnetometer (Quantum

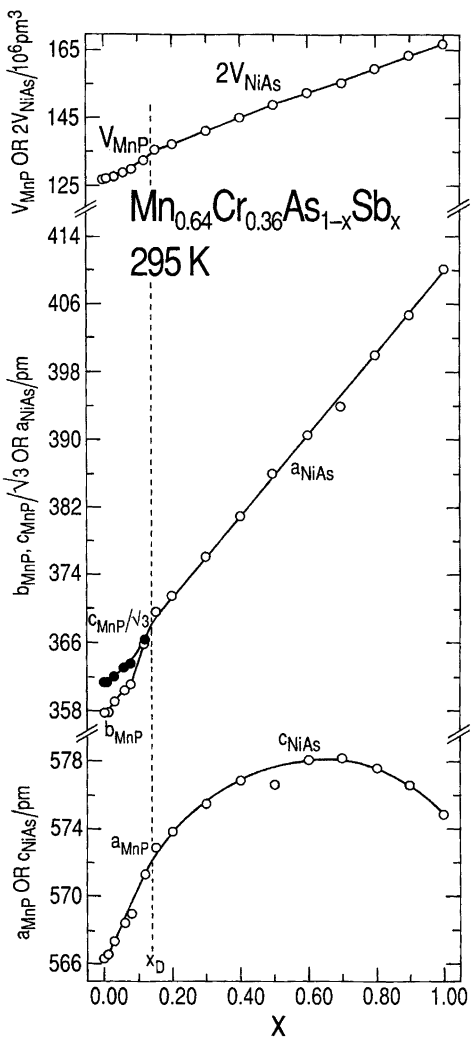

Fig. 1. Variation of unit-cell dimensions for $Mn_{0.64}Cr_{0.36}As_{1-x}Sb_x$ at 295 K. Calculated standard deviations do not exceed size of symbols. Dotted line indicates border between MnP- and NiAs-type structural regimes.

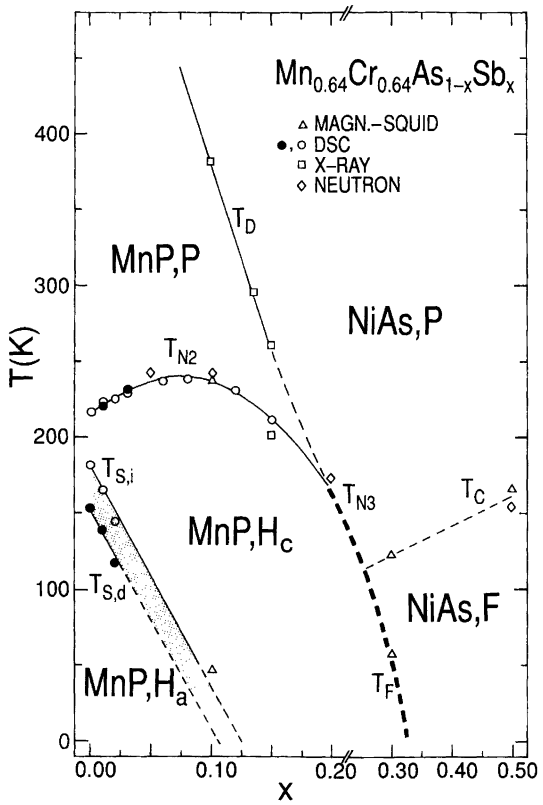

Fig. 2. Structural and magnetic phase diagram for $Mn_{0.64}Cr_{0.36}As_{1-x}Sb_x$. Symbols identifying methods used to determine phase boundaries are given on the illustration, open and filled symbols representing increasing and decreasing temperature conditions, respectively. P paramagnetic, H_c helimagnetic (propagation along ***c***), H_a helimagnetic (propagation along ***a***) and F ferromagnetic. Dotted line is uncertain. Thin lines represent second-order transitions, thicker line and shaded field first-order transitions.

Design; data measured upon heating in a 50 Oe magnetic field). Saturation magnetization was measured at 5 K in fields up to 55 kOe, and was deduced from the measured magnetizations by $1/H$ extrapolation. For the NiAs/F-type state, the inflection point of the $\chi(T)$ curve was used to determine T_C.

Results and discussion

(i) Crystal structure and structural phase transitions. The pseudobinary $Mn_{0.64}Cr_{0.36}As$ end member of the $Mn_{0.64}Cr_{0.36}As_{1-x}Sb_x$ solid-solution phase takes the MnP-type structure at 295 K. The other end member, $Mn_{0.64}Cr_{0.36}Sb$, takes the NiAs-type structure. The variation of the unit-cell dimensions for the complete solid-solution phase is shown in Fig. 1. The unit-cell volume (expressed as V_{MnP} or $2V_{NiAs}$) expands considerably on substitution of As by Sb; $\Delta V/\Delta x \approx 38 \times 10^6$ pm^3 for the composition ranges $0.00 \leqslant x \leqslant 0.10$ and $0.15 \leqslant x \leqslant 1.00$, where the $V(x)$ relationship is linear. For $0.10 < x < 0.15$ there is a larger volume increase, owing to the continuous MnP$\rightleftharpoons$NiAs-type transition. As expected, the Sb substituent simulates a negative chemical pressure (see section iii) which favours the more symmetric (and open) NiAs-type structure relative to the distorted MnP-type structure.[21] As a consequence, T_D decreases from about 700 K for $x=0.00$ to 295 K for $x_D=0.135\pm0.015$. The composition dependence of T_D (Fig. 2) was determined from low- and high-temperature PXD data. For $0.00 \leqslant x \leqslant 0.135$, high-temperature PXD shows a normal MnP$\rightleftharpoons$NiAs-type transition with continuous variation of the $(c/b)_{MnP}$ ratio. The low-temperature PXD data for $x=0.15$ shows a more complex behaviour; line broadening (partial splitting) of some reflections occurs around 260 K and vanishes on further cooling around 200 K. The broadening definitely proves that the onset of the NiAs$\rightleftharpoons$MnP-type transition takes place and fixes $T_D=260$ K. The vanishing broadening at $T=200$ K concurs with the onset of magnetic order, and $(c/b)_{MnP} \approx \sqrt{3}$ is actually an indicator of the H_c-type ordering.

The MnP- and NiAs-type unit cells (described in space groups *Pnma* and $P6_3/mmc$, respectively) are related by $\boldsymbol{a}_{MnP} = \boldsymbol{c}_{NiAs}$, $\boldsymbol{b}_{MnP} = \boldsymbol{b}_{NiAs}$, $\boldsymbol{c}_{MnP} = 2\boldsymbol{a}_{NiAs} + \boldsymbol{b}_{NiAs}$ and $V_{MnP} = 2V_{NiAs}$. The structural changes in terms of $|c/b - \sqrt{3}|$ and atomic coordinates brought about by the Sb substitution are in line with the second-order nature of the MnP$\rightleftharpoons$NiAs-type displacive transition (discussed in terms of Landau theory and group–subgroup symmetry

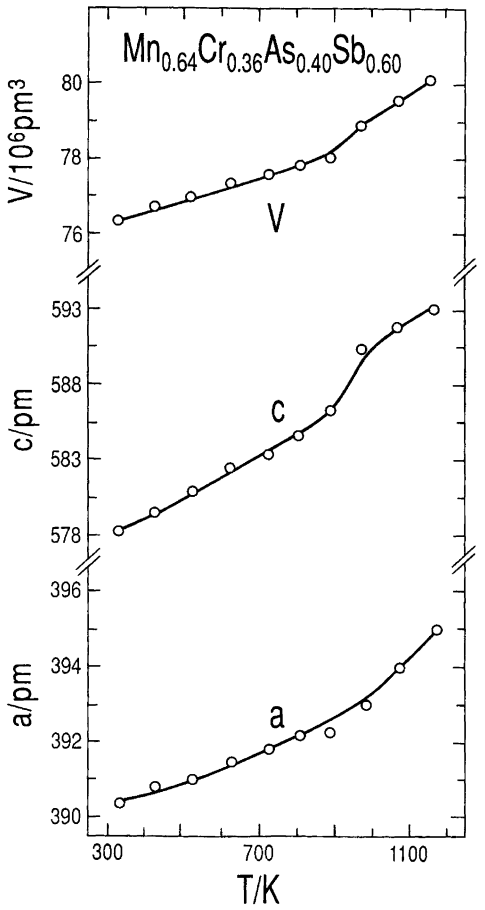

Fig. 3. Temperature variation of the unit-cell dimensions for $Mn_{0.64}Cr_{0.36}As_{0.40}Sb_{0.60}$ between 300 and 1200 K.

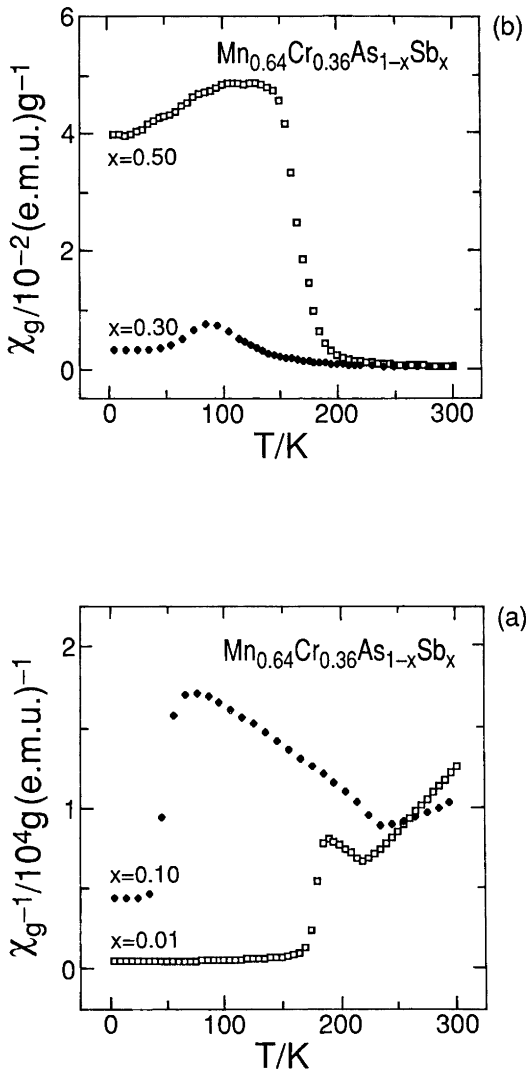

Fig. 4. (a) Inverse magnetic susceptibility versus temperature for $Mn_{0.64}Cr_{0.36}As_{1-x}Sb_x$, $x=0.01$, 0.10 and (b) magnetic susceptibility versus temperature for $x=0.30$ and 0.50.

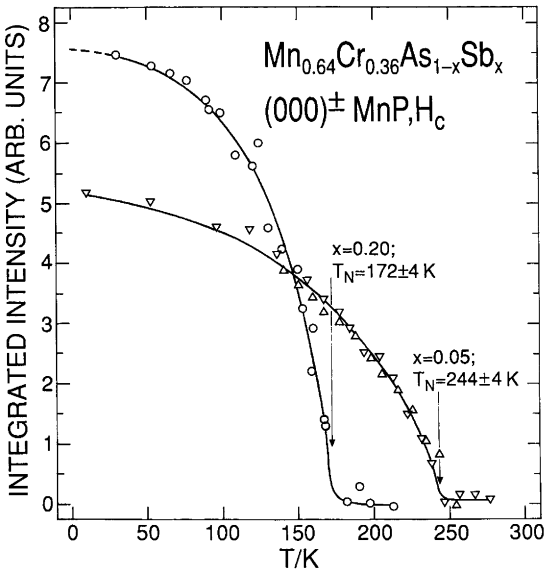

Fig. 5. Temperature dependence of the integrated intensity of (000)± for $Mn_{0.64}Cr_{0.36}As_{0.95}Sb_{0.05}$ and $Mn_{0.64}Cr_{0.36}As_{0.80}Sb_{0.20}$.

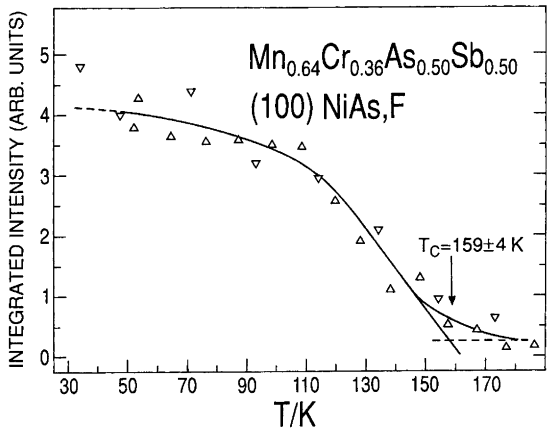

Fig. 6. Temperature dependence of the integrated intensity of (100) for $Mn_{0.64}Cr_{0.36}As_{0.50}Sb_{0.50}$.

considerations in Ref. 22). At 295 K $|c/b-\sqrt{3}|$ decreases towards zero at x_D (Fig. 1). Also the internal distortion becomes progressively smaller, viz. the variable x and z coordinates (4*c* positions) approach the values for the non-distorted NiAs-type state ($x=0$, $z=1/4$ for T and $x=1/4$, $z=7/12$ for X). This is illustrated by the refined atomic coordinates (PND data at 15 K) for $Mn_{0.64}Cr_{0.36}As_{0.80}Sb_{0.20}$: $x_T=0.005\pm0.009$, $z_T=0.207\pm0.005$, $x_X=0.218\pm0.001$ and $z_X=0.586\pm0.003$, compared with those for $Mn_{0.64}Cr_{0.36}As$ (with $x_T=0.016\pm0.007$, $z_T=0.202\pm0.004$, $x_X=0.203\pm0.001$ and $z_X=0.579\pm0.003$). The temperature dependence of the shifts in the atomic coordinates on approaching T_D, in particular Δz_T and Δx_X, has been described in detail for the isostructural phase $MnAs_{0.90}P_{0.10}$.[23]

At 295 K, the unit-cell volume and a_{NiAs} increase linearly with the Sb content x (apart from a range around x_D), whereas c_{NiAs} goes through a maximum around $x=0.65$ (Fig. 1). The $(c/a)_{NiAs}$ ratio decreases from 1.56 for $x=0.15$ to 1.40 for $x=1.00$. This variation may possibly be induced by changes in the magnetic properties, since the Sb-rich samples are ferro- or ferrimagnetically ordered at 298 K.

For $x>x_D$, the NiAs-type phase prevails at 295 K. Rietveld-type refinements of PND data for $x=0.20$ and 0.50 at 295 K verified the NiAs-type structure, with Mn and Cr randomly distributed over the 2*a* site, and correspondingly Sb and As over the 2*d* site (nuclear reliability factor, $R_N=4.5$–5.5). Both sites were fully occupied, whereas the 2*c* site is unpopulated, implying that the stoichiometry is maintained at the 1:1 ratio between T and X. No attempts were made to study the non-stoichiometry for the solid–solution system; however, for the end-phase $Mn_{0.64}Cr_{0.36}Sb$ there are indications for a homogeneity region with $T:X>1$.[24] High-temperature PXD data show significant intensity changes

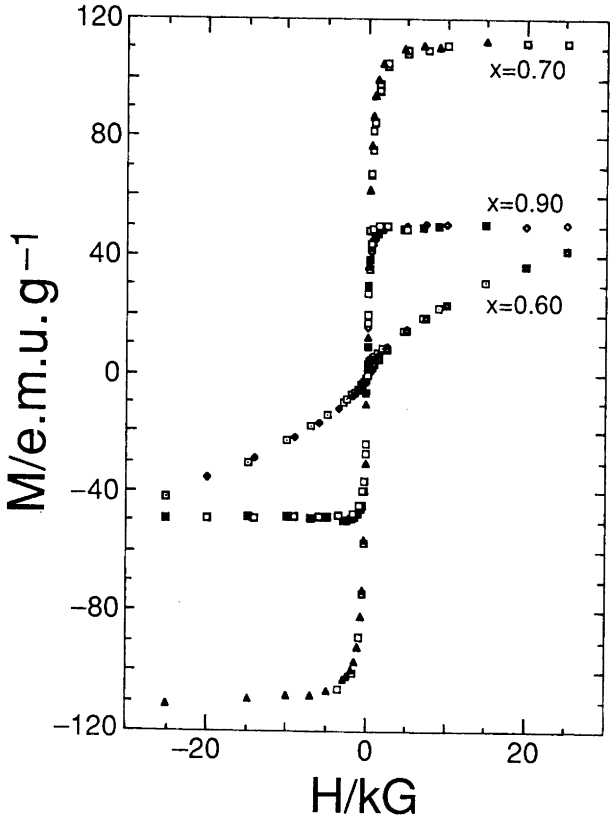

Fig. 7. Magnetization curves for $Mn_{0.64}Cr_{0.36}As_{1-x}Sb_x$ with $x=0.60$, 0.70 and 0.90 at 4.2 K and magnetic fields $-30 \leqslant H \leqslant 30$ kOe.

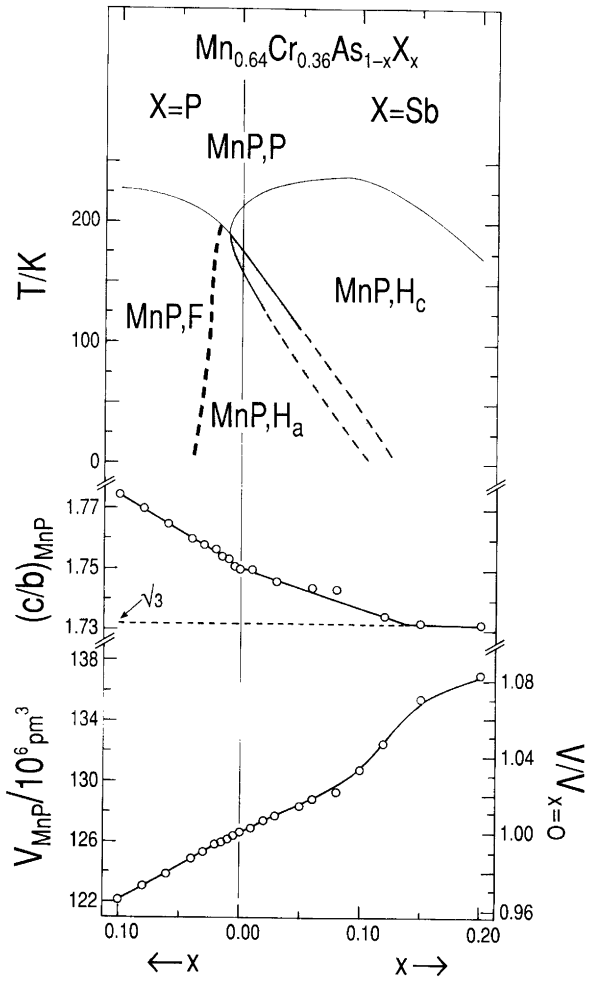

Fig. 8. Sketched magnetic phase-diagram portions, structural deformation in terms of $(c/b)_{MnP}$ and unit-cell volume (at 295 K) for $Mn_{0.64}Cr_{0.36}As_{1-x}X_x$ (X=P, $0.00 \leqslant x \leqslant 0.10$; and X=Sb, $0.00 \leqslant x \leqslant 0.20$).

and variations in the unit-cell dimensions around 1000 K (i.e. around the temperature chosen for the final two-weeks' annealing) for $Mn_{0.64}Cr_{0.36}Sb$ and $Mn_{0.64}Cr_{0.36}As_{0.40}Sb_{0.60}$ (Fig. 3). Simulation of diffraction patterns indicate that the change may imply redistribution of T atoms between octahedral and trigonal bipyramidal sites.

(ii) Magnetic structures and phase diagram. $Mn_{0.64}Cr_{0.36}As$ has two different ordered magnetic states (Fig. 2) as a function of temperature.[1,15] In the temperature intervals $T_{S,i}=175 \leqslant T \leqslant 217$ K $=T_{N2}$, the helimagnetic H_c-type double-spiral structure exists, with propagation direction along $\boldsymbol{c}_{MnP}$ and magnetic moments rotating in the $(ab)_{MnP}$ plane.[1] For $T \leqslant T_S$, the H_a-type double spiral occurs, with propagation along $\boldsymbol{a}_{MnP}$ and moments rotating in the $(bc)_{MnP}$ plane.[1] Substitution of As by Sb changes the magnetic behaviour drastically.

The phase boundaries between the different magnetic phases were determined from PXD, PND, DSC and magnetization measurements (Fig. 2). Representative magnetic susceptibility and inverse magnetic susceptibility curves are shown in Fig. 4.

The magnetic phase diagram for $Mn_{0.64}Cr_{0.36}As_{1-x}Sb_x$ contains (at least) four magnetically ordered phases; H_c, H_a, F and a ferrimagnetic phase, here denoted C (=canted). Substitution of Sb increases the stability region of the H_c-type mode (Fig. 2) on the expense of the H_a-type mode. The H_c- to H_a-type phase boundary (T_S) approaches zero for $x \approx 0.11$. The hysteresis accompanying the transition remains fairly unchanged. T_{N2} goes through a broad maximum around $x \approx 0.08$ (Fig. 2). At substitution levels above $x \approx 0.30$, the samples are ferromagnetically ordered at $T < T_C$ (Fig. 2). For $x=1.00$, a ferrimagnetic structure (C) occurs.[24–27]

The magnetic disorder–order transitions MnP,P- to MnP,H_c-type (at T_{N2}) and NiAs,P- to NiAs,F-type (at T_C) are of second order. The situation is more unclear for the NiAs,P- to MnP,H_c-type transition (at T_{N3}). PXD films, covering the latter transition, show no discontinuities in the Bragg positions. Possibly, both the magnetic ordering and the structural distortion (at T_D) occur as second-order processes in a narrow temperature interval. The order–order transitions MnP,H_c- to MnP,H_a- (at T_S) and MnP,H_c- to NiAs,F-type (at T_F) are of first order. The joining of T_D and T_{N2} into T_{N3} resembles the situation for $CrAs_{1-x}Sb_x$, where the MnP,H_c-type phase

from the CrAs side meets the NiAs,AF-type phase from the CrSb side.[28]

The incommensurate H_c-type magnetic structure is manifested by satellite reflections around the nuclear reflections in the PND diagram, and for $x=0.20$ they define the propagation vector $\tau_c=0.259\times 2\pi c^*$ at 20 K. The magnetic moment (μ_H) and the phase angle (ϕ) were derived from individual satellite intensities by the program SPIRAL.[21] For $x=0.20$ the values $\mu_H=1.95\pm0.10\mu_B$ and $\phi=-150\pm5°$ are close to those found for $Mn_{0.63}Cr_{0.37}As$.[1] From the temperature dependence of the integrated intensity of the $000^{\pm}$ satellite reflection,

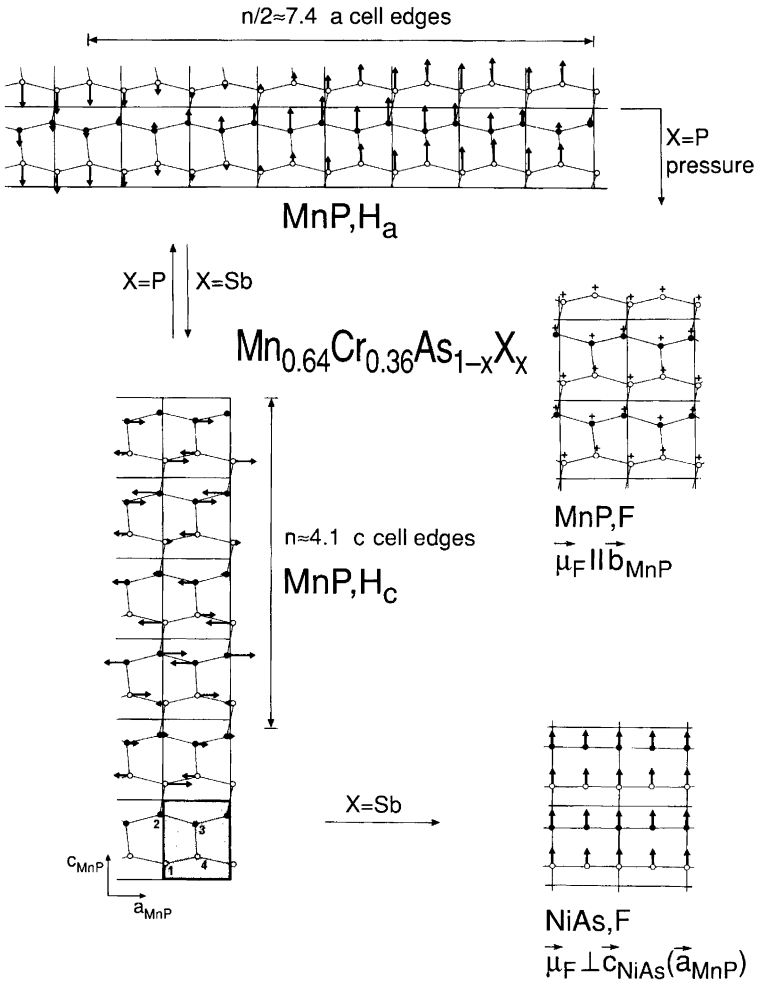

Fig. 9. Magnetic structures occurring for the $Mn_{0.64}Cr_{0.36}As_{1-x}X_x$ solid solution phase (X=P, Sb). For H_c-type order, magnetic moments are within $(ab)_{MnP}$-plane, for H_a-type order magnetic moments are within $(bc)_{MnP}$-plane, for NiAs,F-type order magnetic moments are within the basal plane $(ab)_{NiAs}$ and for MnP,F-type order magnetic moments are parallel to b_{MnP} (indicated by + on the illustration).

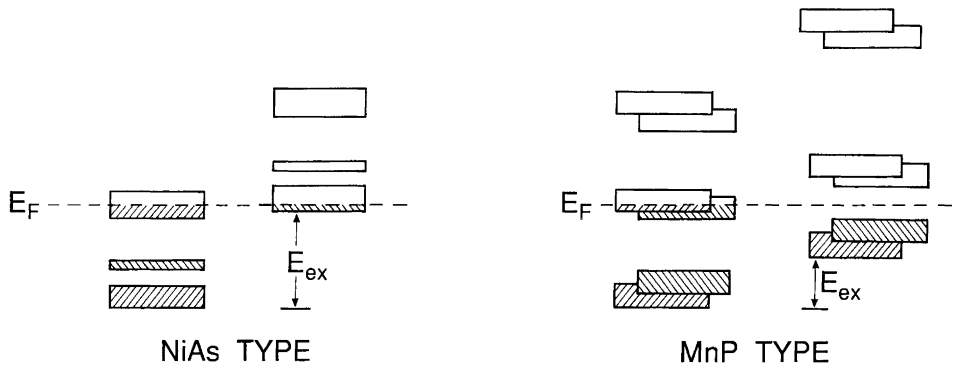

Fig. 10. Schematic band-structure diagram for MnAs (hexagonal, high spin and orthorhombic, low spin) based on Ref. 30.

$T_{N2}=172\pm4$ K [Fig. 5, where also the corresponding plot for $x=0.05$ ($T_{N2}=244\pm4$ K) is included].

The PND pattern for $Mn_{0.64}Cr_{0.36}As_{0.50}Sb_{0.50}$ at 20 K is consistent with a simple NiAs-type crystal structure; however, several of the fundamental reflections have gained additional intensity due to magnetic contributions. The magnetic ordering temperature $T_C=159\pm5$ K was determined from the temperature dependence of the integrated intensity of (100) (Fig. 6). From Rietveld-type refinements, the magnetic ordering was found to be ferromagnetic with the moments, $\mu_F=1.69\pm0.09\mu_B$, located within the basal $(ab)_{NiAs}$ plane ($R_N=4.9$, $R_M=6.8$).

The fully substituted end phase $Mn_{0.64}Cr_{0.36}Sb$ ($x=1.00$) is, according to published phase-diagram data, antiferromagnetically ordered.[24-27] Present PND data for $Mn_{0.64}Cr_{0.36}Sb$ at 295 K show a canted magnetic structure with the AF component within the $(ab)_{NiAs}$ plane, $\mu_{AF}=2.96\pm0.14\mu_B$, and a ferromagnetic component, $\mu_F=1.11\pm0.06\mu_B$, parallel to c_{NiAs}. DSC data gave an ordering temperature of 380 ± 2 K.

Magnetization and magnetic hysteresis curves at 4.2 K for Sb-rich samples of $Mn_{0.64}Cr_{0.36}As_{1-x}Sb_x$ are shown in Fig. 7. The saturation moment increases from $1.81\mu_B$ for $x=0.40$ to $3.42\mu_B$ for $x=0.70$. For samples with higher Sb contents, the saturation moment decreases and equals $1.58\mu_B$ for $x=0.90$. This behaviour confirms that the most Sb-rich samples are in a ferrimagnetic state (C) and that saturation of the antiferromagnetic component is not reached at 50 kOe. The $M(H)$ curves at 4.2 K are sigmoidally shaped for the Sb-poor, NiAs,F-type samples, whereas step-like curves were obtained for Sb-rich samples (Fig. 7). The remanence and coercivity for the ferromagnetic part of the samples with $0.40\leqslant x\leqslant1.00$ are very small.

(iii) Chemical pressure. As described, the structural and magnetic properties of $Mn_{0.64}Cr_{0.36}As$ are strongly influenced by P or Sb substitution. Figure 8 correlates the variation of the structural deformation in terms of $(c/b)_{MnP}$, the unit-cell volume and magnetic phase-diagram data at low substitution levels ($x_P\leqslant0.10$ and $x_{Sb}\leqslant0.20$). Note that for the $\Delta x=0.10$ substitution interval, the volume changes $\Delta V/\Delta x$ introduced by P and Sb substitution are of equal magnitude, but of opposite sign.

The different magnetic structures of As-rich $Mn_{0.64}Cr_{0.36}As_{1-x}X_x$ (X=P, Sb) are illustrated in Fig. 9. According to Fig. 8, increased unit-cell volume correlates with transitions from the MnP,F- via MnP,H_a- and MnP,H_c- to the NiAs,F-type. The opposite phase sequence is expected to be found for studies of samples with moderate Sb-contents when subjected to external pressures.[14,15]

Electronic band-structure calculations, including spin-polarized calculations, are available for MnAs.[29] However, schematic diagrams have frequently been used to picture the electronic band structure. Two such schemes, for NiAs-type high-spin MnAs[30,31] and MnP-type low-spin MnAs,[30] are shown in Fig. 10. The Fermi energy (E_F) is situated in broadened d-bands between bonding and antibonding sp-bands. Manganese and chromium in $Mn_{0.64}Cr_{0.36}As_{1-x}X_x$ (for x small; say $x\leqslant0.20$) have a 'low' magnetic moment (which indicates that the exchange splitting, E_{ex}, is less than the crystal-field splitting, E_{cf}) and the deviation from values for the free ions are in accordance with the metallic properties of the phase. Substitution of As by P or application of an external pressure, increases the structural deformation of the (Mn,Cr)X_6 octahedron by splitting the originally (for the NiAs-type case) six equivalent T–X bond distances into four (2+2+1+1) and reducing the T–T separations. The two nearest T–T neighbours are $d_{1,4}=291.1$ pm apart, the two next-nearest neighbours are separated by $d_{1,2}=323.4$ pm and the two next-next-nearest neighbours by $d_{1,1}=b_{MnP}=370.9$ pm for X=Sb, $x=0.20$ and $T=20$ K. These are reduced to, respectively, 285.0, 305.6 and 345.1 pm for X=P, $x=0.05$ and $T=10$ K. In the same process, the average T–X bond distance for the deformed octahedron is reduced from 259.1 to 249.2 pm. The effect of P and Sb substitution in $Mn_{0.64}Cr_{0.36}As$ on these interatomic distances are quite opposite. The crystal-field splitting is mainly influenced by the (Mn,Cr)–X bond distances (which actually are well reflected by the unit-cell volume), whereas the exchange splitting is mainly influenced by the broadening of d-bands via T–T interactions. $d_{1,2}$ shows by far the largest variation for the present solid-solution phase and decreases from 323.4 pm for $Mn_{0.64}Cr_{0.36}As_{0.80}Sb_{0.20}$ to 305.6 pm for $Mn_{0.64}Cr_{0.36}As_{0.95}P_{0.05}$ (at 20 K). It is hence inferred that P-substitution implies larger E_{cf}, broader bands and smaller E_{ex}. Sb-substitution on the other hand, leads to smaller E_{cf}, narrower d-bands and larger E_{ex}. The equivalence between chemical pressure (positive or negative) and external pressure is conceivable on this background. In MnAs and its solid-solution derivatives, applied external pressure causes shortening of the T–X bonds and a drastic reduction of the T–T bonds follows upon increasing structural distortion. Similar equivalence considerations are expected to hold in other metallic solid-solution systems, in particular where essential characteristics of the electronic band structure are similar to those of MnAs.

Acknowledgement. This work has obtained financial support from the Research Council of Norway.

References

1. Fjellvåg, H. and Kjekshus, A. *Acta Chem. Scand., Ser. A 38* (1984) 1.
2. Fjellvåg, H. and Kjekshus, A. *Acta Chem. Scand., Ser. A 39* (1985) 671.
3. Andresen, A. F., Bärner, K., Fjellvåg, H., Heinemann, K., Kjekshus, A. and Sondermann, U. *J. Magn. Magn. Mater. 58* (1986) 287.
4. Andresen, A. F., Fjellvåg, H., Kjekshus, A. and Lebech, B. *J. Magn. Magn. Mater. 62* (1986) 247.
5. Zięba, A., Zach, R., Fjellvåg, H. and Kjekshus, A. *J. Phys. Chem. Solids 48* (1987) 79.

6. Komada, N., Westrum, E. F., Fjellvåg, H. and Kjekshus, A. *J. Magn. Magn. Mater. 65* (1987) 37.
7. Zięba, A., Fjellvåg, H. and Kjekshus, A. *J. Magn. Magn. Mater. 68* (1987) 115.
8. Fjellvåg, H., Kjekshus, A. and Zięba, A. *J. Magn. Magn. Mater. 67* (1987) 354.
9. Fjellvåg, H., Kjekshus, A. Stølen, S. and Andresen, A. F. *Acta Chem. Scand., Ser. A 42* (1988) 214.
10. Fjellvåg, H. Grønvold, F., Kjekshus, A. and Stølen, S. *J. Solid State Chem. 75* (1988) 355.
11. Schünemann, J.-W., Bärner, K., Fjellvåg, H., Kjekshus, A., Eigemann, J., Gmelin, E. and Sondermann, U. *Phys. Stat. Solidi (a) 110* (1988) 141.
12. Zięba, A., Zach, R., Fjellvåg, H. and Kjekshus, A. *J. Phys. 49* (1988) C8–203.
13. Fjellvåg, H., Karen, P., Kjekshus, A., Zięba, A., Chattopadhyay, T. and Vettier, C. *J. Magn. Magn. Mater. 92* (1990) 75.
14. Andresen, A. F., Bärner, K., Fjellvåg, H., Kjekshus, A., Rager, H., Sondermann, U. and Stølen, S. *J. Magn. Magn. Mater. 94* (1991) 347.
15. Zięba, A., Fjellvåg, H., Kjekshus, A. and Zach, R. *Phys. Rev. B 44* (1991) 196.
16. Ersson, N. O., *Program CELLKANT*, Chemical Institute, Uppsala University, Uppsala, Sweden 1981.
17. Hewat, A. W. *The Reitveld Computer Program for the Profile Refinement of Neutron Diffraction Powder Patterns Modified for Anisotropic Thermal Vibrations*, UKAERE Harwell Report RRL 73/897, Harwell 1973.
18. Rietveld, H. M. *J. Appl. Crystallogr. 2* (1969) 65.
19. Koester, L. and Yelon, W. B. In: Yelon, W. B., Ed., *Neutron Diffraction Newsletter*, The Neutron Diffraction Commission, Missouri 1983.
20. Watson, R. E. and Freeman, A. F. *Acta Crystallogr. 14* (1961) 27.
21. Fjellvåg, H. and Kjekshus, A. *Acta Chem. Scand., Ser. A 40* (1986) 8.
22. Franzen, H. F., Haas, C. and Jellinek, F. *Phys. Rev. B 10* (1974) 1248.
23. Fjellvåg, H., Kjekshus, A. and Stølen, S. *J. Solid State Chem. 64* (1986) 123.
24. Takei, W. J., Cox, D. E. and Shirane, G. *Phys. Rev. 129* (1963) 2008.
25. Bouwma, J., van Bruggen, C. F. and Haas, C. *J. Solid State Chem. 7* (1973) 255.
26. Grazhdankina, N. P., Bersenev, Y. S. and Zainullina, R. I. *Zh. Eksp. Teor. Fiz. 87* (1984) 537 [Eng. transl. *Sov. Phys. JETP 60* (1984) 307].
27. Reimers, W., Hellner, E., Treutmann, W., Brown, P. J. and Heger, G. *J. Magn. Magn. Mater. 15–18* (1980) 479.
28. Kallel, A., Boller, H. and Bertaut, E. F. *J. Phys. Chem. Solids 35* (174) 1139.
29. Sandradskii, L. M., Egorov, R. F. and Berdyshev, A. A. *Phys. Stat. Solidi (b) 103* (1981) 511.
30. Menyuk, N., Kafalas, J. A., Dwight, K. and Goodenough, J. B. *Phys. Rev. 177* (1969) 942.
31. Haneda, S., Kazama, N., Yamaguchi, Y. and Watanabe, H. *J. Phys. Soc. Jpn. 42* (1977) 1201.

Received November 28, 1996.